PHYSICAL REVIEW B **78**, 024112 (2008)

Metastability of multitwinned Ag nanorods: Molecular dynamics study

J. Monk,[1] J. J. Hoyt,[2] and D. Farkas[1]
[1]*Department of Materials Science, Virginia Tech, Blacksburg, Virginia 24061, USA*
[2]*Department of Materials Science and Engineering, McMaster University, Hamilton, Ontario, L8S 4K1 Canada*
(Received 9 January 2008; revised manuscript received 18 June 2008; published 16 July 2008)

Nanoscale rods have been shown to exhibit a multiple twinned structure. The rods grow along a [110]-type crystallographic direction and have a pentagonal cross section with five (111) twins connecting the wire center to the corners of the pentagon. Here, we use molecular dynamics simulations with an embedded atom method interatomic potential for Ag to compute the ground-state energies of the multitwinned rods and compare with the bulk equilibrium crystal shape, as estimated from a Wulff construction. The excess energy of the nontwinned equilibrium nanorods and the multitwinned nanorods was obtained as a function of the wire length (L) as well as the cross sectional area (A_{cs}). Various contributions to the total energy, such as twin boundary energy and surface energies, are discussed and included in an analytical model that compares favorably with the simulation results. Our results show that for infinitely long nanowires with $A_{cs} < 1500$ nm^2, the nontwinned structure is always energetically favorable. However, if the energy of the dipyramidal atomic structure at the nanorod ends is included in the model then the twinned nanorods are stable with respect to the nontwinned rods below a critical aspect ratio ($L/\sqrt{A_{cs}}$).

DOI: 10.1103/PhysRevB.78.024112 PACS number(s): 64.70.Nd, 62.23.Hj, 61.72.Mm, 61.46.−w

I. INTRODUCTION

In recent years, interest in metallic nanowires has grown because of the possible application to nanomechanical and nanoelectronic devices. Metal nanowires exhibit desirable properties such as superior strength,[1,2] excellent conductivity,[3] and good optical properties.[4–6] The current study focuses on silver (Ag) nanowires, which have great potential for higher strengths due to the existence of multiple twinned structures.[7–11] The increased strength in the multitwinned nanorods has been attributed to the twinned structure's ability to hinder dislocation motion and generate work hardening in the material.[1,12]

Multitwinned particulates are used as seeds to grow multitwinned nanorods (MTRs) and have been observed for over half a century starting with their discovery by Ino in 1966.[13] However, the growth mechanisms of MTRs were poorly understood until recent years.[14–21] The MTR which is the focus of the present work is the fivefold "star" nanorod, which, in cross section, consists of five (111) twins connecting the corners of the pentagon to the center of the wire. The unique characteristics of these fivefold twinned nanorods are not seen at the micrometer scale as the rods require extra elastic energy to produce the pentagonal shape. Elastic strain (energy) is generated from the small difference in a twin boundary angle of 70.5° and the 72° angle is required to create a pentagon from the five twins.

A number of previous studies have attempted to characterize the elastic strain and/or extended defects necessary to accommodate the total 7.5° gap in the MTR structure. Hofmeister *et al.*[9] used high-resolution transmission electron microscopy (HRTEM) to study elastic strains in Ag and Au nanowires with lengths in the range of 22–132 nm and aspect ratios of 1.8–6.0. The authors observed no extended defects and instead found nonuniform lattice distortions beneath the prism surface. Chen *et al.*[10] used HRTEM to study the structure of Ag nanowires and found a well-defined coherent twinning relationship for two of the five twins of the star. In a study particularly relevant to the present work, Ding *et al.*[22] included the elastic strain in an analytic model for the total energy of an MTR and found that the elastic contribution is small for nanowire radii less than several tens of nanometers. The authors also compared the energies of MTR with the energy of six-sided bulk nanowires and found, somewhat surprisingly, that the twinned nanowire structure was metastable. The study of Ding *et al.*[22] demonstrated that not only the mechanism of elastic strain accommodation in MTR's is poorly understood but also the problem of thermodynamic stability has not been settled in the case of small size nanowires where the elastic contribution is negligible.

Our study incorporates experimental and analytical results for the microstructure of the MTRs and builds upon their findings to discover what factors affect the stability of the MTRs. For this purpose, we used molecular statics and dynamics simulations in combination with an analytical model to study the stability of fivefold star nanorods in comparison to the nontwinned "bulk" shape defined by a Wulff construction[23] for various lengths and cross-sectional areas. Based on the atomistic results, we designed an analytical model similar to Ding *et al.*[22] which accounts for the geometry, surface, twin, and elastic energies of the nanorods. The analytical model was developed for the twinned and nontwinned nanorods with and without considering the atomic structure at the rod ends. We use the analytical model and simulation output to describe the relative stability of the rods and find a critical aspect ratio, defined as $L/\sqrt{A_{cs}}$, below which the multitwinned nanorods are stable.

II. GENERATION OF MOLECULAR DYNAMICS SIMULATION CELLS

A. Wulff construction for the nontwinned nanorods

The nontwinned bulk equilibrium microstructure was determined using a Wulff construction, as shown in Fig. 1. The

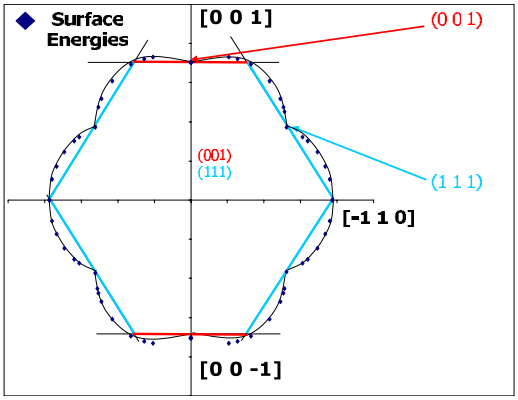

FIG. 1. (Color online) Wulff Construction for the Voter-Chen EAM Potential for Ag.

silver nanorods observed in experiments grow along the ⟨110⟩-type axis and therefore the surfaces included in the Wulff plot are all perpendicular to the [110] axis. We expect an equilibrium shape similar to the structure produced by Marks[23] in 1984. For each surface, Table I shows the angles θ_{hkl} of the surface normal with respect to the $[1\bar{1}0]$ direction, and the corresponding surface energies calculated using the interatomic potential of Voter and Chen[24] selected for our simulation. Based on these values, the Wulff construction indicates that the bulk equilibrium nanostructure has six surfaces made up of four low energy (111) planes and two (001) plane surfaces. The surface energies for the Voter and Chen embedded atom method (EAM) potential, γ, are shown in Table I and the cusps in the Wulff plot correspond to the {111}- and {001}-type surfaces, are shown in bold in Table I. The surface energy of the lowest energy plane {111} is 1.6055 J/m^2 and {001} has a surface energy of 1.7593 J/m^2

TABLE I. Surface energies γ (J/m^2) for various orientations observed for the Voter-Chen Potential. Theta angles are taken with respect to $[1\bar{1}0]$.

[*hkl*]	θ (*hkl*) (rad)	Silver γ_{hkl}
[0 0 1]	1.57	1.7593
[1 −1 5]	1.85	1.8975
[1 −1 4]	1.91	1.9126
[−1 1 3]	2.01	1.9209
[−1 1 2]	2.19	1.8642
[−2 2 −3]	2.33	1.7810
[−3 3 4]	2.39	1.7360
[−4 4 −5]	2.42	1.7090
[−1 1 −1]	2.53	1.6055
[−4 4 −3]	2.65	1.7281
[−3 3 −2]	2.70	1.7663
[−2 2 −1]	2.80	1.8353
[3 −3 1]	2.91	1.8901
[−5 5 −1]	3.00	1.9190
[−1 1 0]	3.14	1.9342

with a ratio of 1.0958. The use of the Voter-Chen Ag EAM potential is justified by the good agreement of the surface energy ratio with the first-principle results for silver, 1.1053.[25]

B. Multitwinned structure

The multitwinned nanorods observed by Yacaman *et al.*[11] exhibited a pentagonal shape with five twins in a star formation. A model of the fivefold nanorod is shown in Fig. 2. As discussed above, there exists a 7.5° gap produced by the difference in the (111) twin boundary angle and the geometric constraint of a pentagon and the mismatch introduces elastic energy in the system. The existence of this elastic strain implies an upper size limit of the MTR. There have been a few hypotheses for how the MTR system distributes the elastic strain in the nanorod to accommodate for the 7.5°.[12,20] To generate the initial nanorod geometry in our studies, we have chosen to strain the atoms along the x axis, as seen in Fig. 2. Confining the elastic strain in one direction allows us to simplify the equations used to define the strain in the system. The strain is defined as $b-b_o/b_o$, where b_o is the base of the 35.25° triangle and b is the base of the 36° triangle.

The relationship between the base of the 35.25° triangle and the 36° triangle is

$$b = \frac{\tan(36°)}{\tan(35.25°)} b_o. \tag{1}$$

The atomic displacement of each atom is shown in Fig. 2 and given by

$$X = \left[\left(1 - \frac{b_o - \Delta X}{b_o} \right) * (b - b_o) \right] X_o, \tag{2}$$

where X is the atomic displacement of each atom, ΔX is the distance in the x axis from the center of the pentagon, and X_o is the initial position of the atom in the x axis. Note that central atoms (X_c) are located at $X_c=0$ and $\Delta X=(X_o-X_c)=X_o$. Equation (2) shows that atoms further away from central atoms will have more displacement, those closer to central atoms will have small displacements, generating a "stretched" triangle. The maximum amount an atom will be displaced is $X_o=b_o$, thus resulting in a distance of $X_{\max}=0.028*X_o$. The stretched triangle obtained by this method is then rotated about point A as in Fig. 2 until the full pentagon is created and all overlapping atoms are removed. The radius can easily be increased to create larger MTR with different cross-sectional areas. The cross sections of the twinned and nontwinned nanorods are shown in Fig. 3.

III. SIMULATION TECHNIQUES

The atomic interactions of the virtual Ag samples were governed by a Voter-Chen EAM potential[24] (Sec. VII briefly describes results from two additional Ag EAM potentials). Simulations to find the energy of the nanorod structures were performed using the multiprocessor molecular statics and dynamics software LAMMPS created by Plimpton.[26] For the dy-

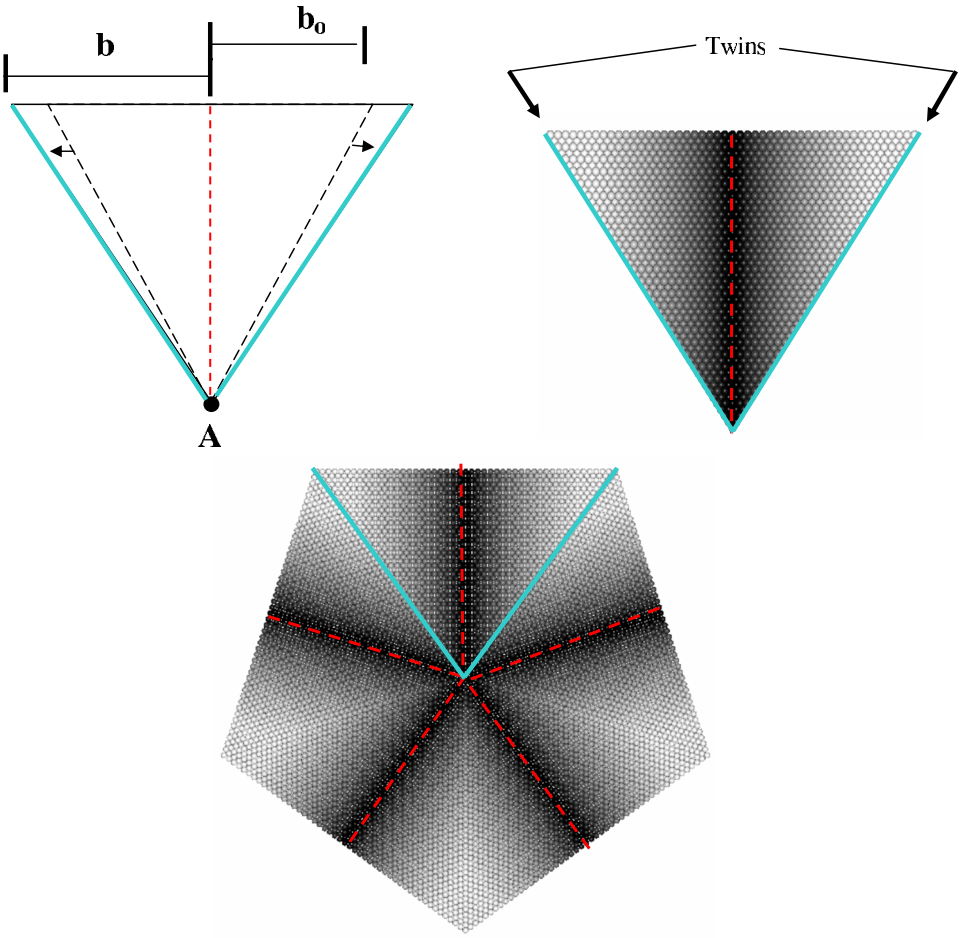

FIG. 2. (Color online) DOE. (a) shows the compensation for the 7.5°. The dashed triangle is the initial triangle, 70.5°, whereas the solid triangle corresponds to angle of 72°. The top right shows the displacement of each atom, atoms displaced (a) X_{max} are white, atoms displaced (b) 0.0 are black. The arrows indicate the twin boundaries. The bottom figure shows the triangle rotated $2\pi/5$ about point A, this creates the unrelaxed pentagon with displacement coloring. The dashed lines are central atoms with no displacement (red).

namics runs under NPT conditions, the temperature and pressure were controlled by a Nose-Hoover thermostat and barostat, respectively; these conditions allowed atomic movement at the surfaces, and periodic and zero pressure boundaries applied along the nanorod length allowed for stress relaxation due to Poisson contraction. Molecular statics simulations used the conjugate gradient method, which allowed the system to find a minimum in the energy functional.[27]

A series of MD simulations were run at 1 K for 5 ps for each nanorod to allow for relaxation at the surfaces and periodic boundaries. In order to try to achieve a global minimum configuration, and as explained in more detail below, the ground-state energy of the larger nanorods was determined by first performing dynamics simulations at high temperatures and subsequently cooling the system. After the molecular dynamics were completed, the system underwent an energy minimization and the total energy of the nanorod was obtained for the minimum configuration. The excess energy for each nanorod was determined by subtracting the ground-state energy of the bulk material with the same number of atoms from the atomic energies calculated in the simulations. As expected the higher-energy atoms for the MTRs were located at the surface and twins, whereas the nontwinned nanorods contained only high-energy surface atoms which contributed to the excess energy of the system. The excess energy was found for the MTR and the nontwinned nanorods of different cross sections, while the length was kept constant at 3.32 nm (periodic). The cross-sectional areas varied from 7.12 to 1460 nm^2.

It is important to stress that the surface, twin boundary, and elastic energies obtained from molecular statics correspond to the ground state ($T=0$ K). Therefore the conclusions drawn from this study may change slightly at 300 K, which is the actual growth temperature of nanorods.[28] All the surface and twin boundary energies are expected to somewhat change with temperature and there will be entropy contributions to the overall free energy at room temperature, but we still expect our ground-state results to provide a good description for room-temperature behavior. In a thermodynamic integration study of defect energies in EAM Cu, Foiles[29] showed that the decrease in (100) surface energy from the ground state to 300 K is small, roughly 6%. Moreover, the decrease in energy of a $\Sigma 5$ grain boundary follows a similar trend, suggesting that the ratio of free energy for various crystal faces will remain roughly constant with temperature and a ground-state analysis should provide an accurate description of the room-temperature behavior.

IV. ANALYTICAL MODEL OF PERIODIC NANORODS WITHOUT CONSIDERATION OF THE ROD ENDS

A. Multitwinned nanorods

The equation for the excess energy of the multitwinned nanorod must take into account the five (100) surfaces, the

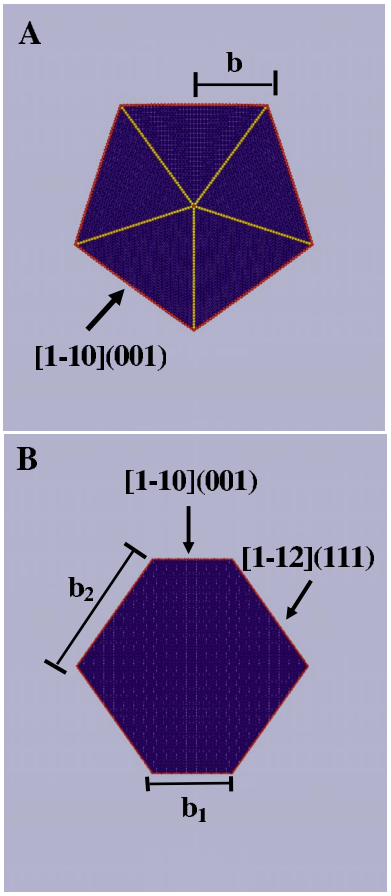

FIG. 3. (Color online) The relaxed microstructures for the (a) multitwinned nanorods and (b) nontwinned nanorods. Coloring by centrosymmetry parameter, gold lines are twin boundaries.

five twin boundaries, and the elastic energy due to the strain that compensates for the 7.5° gap. We first calculated the cross-sectional area as a function of the triangle base length,

$$A_{cs} = 5\frac{b^2}{\tan(\theta_1)}, \tag{3}$$

where A_{cs} is the cross-sectional area, b is the base length of the pentagon, and $\theta_1 = 36°$ or 0.628 rad. Equation (3) is simply the geometric calculation of the area of a pentagon. An analytical representation of the excess energy of the multitwinned nanorods [Eq. (4)] was determined from the surface, twin, and elastic energies and the size dimensions of the rod,

$$\Delta E_{MTR} = \left(\frac{1}{5}\tan(\theta_1)\right)^{1/2}\left(10\gamma_2 + \frac{5\gamma_t}{\sin(\theta_1)}\right)L(A_{cs})^{1/2} + 2U_M L A_{cs}, \tag{4}$$

where L is length of the rod, A_{cs} is cross sectional area, U_M is the elastic energy, γ_2 is the (001) surface energy and γ_t is the twin energy of the system, and $\theta_1 = 0.628$. The first energy term in Eq. (4) identifies the five free surfaces along (001) planes found for the pentagon shape. The surface energy for the (001) plane is given in Table I as $\gamma_2 = \gamma_{001} = 1.76$ J/m^2. The surface energy is multiplied by the surface area, excluding the periodic ends. The twin boundary energy was found to be $\gamma_t = 0.108$ J/m^2 for the Voter-Chen EAM potential[24] and is multiplied by the cross-sectional area and length. The final term is the contribution of the elastic strain in the multitwinned structures. The order of magnitude of this elastic term can be estimated as $U = 1/2G\varepsilon^2$, where ε is the elastic strain of approximately 7.5/360. This term is negligible for very small cross-sectional areas and increases in importance as the cross-sectional areas increase. In the present analytical model we restrict ourselves to small cross sectional areas, for which the elastic energy term can be estimated to be less than 2 orders of magnitude smaller that the contributions of the surface energy. Furthermore, some of the elastic energy can be relieved by the emission of dislocations. We therefore neglect the elastic energy term. The fact that the elastic energy is indeed negligible for $A_{cs} < 1500$ nm^2 was confirmed by the agreement in the energies given by the atomistic simulation and the analytical model, as shown below. We therefore calculate the excess energy of the multitwinned nanorods without the elastic energy term as

$$\Delta E_{MTR} = \left(\frac{1}{5}\tan(\theta_1)\right)^{1/2}\left(5\gamma_2 + \frac{5\gamma_t}{\sin(\theta_1)}\right)L(A_{cs})^{1/2}, \tag{5a}$$

Eq. (5a) illustrates the dependence of the energy on the length (L) and the cross-sectional area (A_{cs}) with the relationship, $L\ (A_{cs})^{1/2}$. A constant K_1 can be defined as

$$K_1 = \left(\frac{1}{5}\tan(\theta_1)\right)^{1/2}\left(5\gamma_2 + \frac{5\gamma_t}{\sin(\theta_1)}\right), \tag{5b}$$

such that

$$\Delta E_{MTR} = K_1 L(A_{cs})^{1/2}, \tag{5c}$$

where $K_1 = 7.05$ when $\gamma_2 = \gamma_{001} = 1.76$ J/m^2 and $\theta_1 = 0.628$ as defined by the Wulff plot.

B. Nontwinned nanorods

To develop the analytical model for the nontwinned nanorods, we calculated the cross-sectional area as a function of the (001) plane length, b_1, and (111) plane length, b_2 [the lengths b_1 and b_2 are shown schematically in Fig. 3(b)]. The area is given by

$$A_{cs} = 2|\cos(\theta_3)|\, b_1 b_2 + 2|\cos(\theta_3)\sin(\theta_3)|b_2^2. \tag{6}$$

Equation (6) shows the relationship of the cross-sectional area, A_{cs}, θ_{111}, and the surface lengths, b_1 and b_2. $\theta_3 = \theta_{111} = 2.53$ rad is given in Table I and is taken with respect to the $[1\bar{1}0]$ orientation.

The analytical model for the nontwinned nanorods introduces two excess energies from the (001) and (111) surfaces as given in Eqs. (7a) and (7b). The excess energy for a nontwinned nanorod of length L is

$$\Delta E_{HEX} = K_2 L A_{cs}^{1/2}, \tag{7a}$$

where a second constant K_2 has been introduced and is defined as

$$K_2 = \frac{2\gamma_2\{[\cos(\theta_2) + \sin(\theta_3)\tan(\theta_3)]\gamma_3 - \sin(\theta_2)\tan(\theta_3)(\gamma_2)\} + 4\gamma_3\left[\frac{\sin(\theta_2)}{\cos(\theta_3)}\gamma_2\right]}{\{\gamma_2 \sin(\theta_2)[4\gamma_3 \sin(\theta_3)\tan(\theta_3) + 4\gamma_3 \cos(\theta_3)] - 2\gamma_2^2[\sin(\theta_2)]^2 \tan(\theta_3)\}^{1/2}}. \quad (7b)$$

With the values $\theta_2 = \theta_{001} = 1.57$ and $\theta_3 = \theta_{111} = 2.53$ and the surface energies found from the Wulff plot $\gamma_2 = \gamma_{001} = 1.7593$ and $\gamma_3 = \gamma_{111} = 1.6055$, we obtain $K_2 = 8.15$.

The final relationship between the excess energy of the nontwinned nanorods seen in Eq. (7a) exhibits the same $L(A_{cs})^{1/2}$ dependence seen in the multitwinned nanorods, as shown in Eq. (5c). When comparing the constants K_1 and K_2, we find that because $K_1 > K_2$, the excess energy of the multitwinned nanorods will *always* be larger than the nontwinned nanorods. This result of the analytical model can be compared with the simulations of the twinned and nontwinned nanorods as shown in Sec. V.

V. SIMULATION RESULTS

Atomistic simulations were performed for a series of cross-sectional areas and periodic boundary conditions applied along the length of the rod. To find the excess energy of the system, we subtracted the energy of the perfect bulk crystal material (−2.85 eV/atom for the VC potential) from the total energy of the structure obtained in the simulation. The excess energy is produced by the higher-energy atoms, such as the surface, twin boundary, and elastically strained atoms. The excess energy of the system was found for each simulation run by using the combination of molecular dynamics and conjugate gradient minimization techniques to calculate the atomic energies for each rod.

Molecular statics and dynamics simulations were run for the MTR and nontwinned nanorods with increasing cross-sectional areas. The length of the nanorods was kept constant with periodic boundary conditions for the ends. The simulation results are consistent with the analytical models in the dependence on the square root of the cross-sectional area, A_{cs}. From the simulation data the excess energies of the multitwinned nanorods are higher than the nontwinned nanorods for all cross-sectional areas, again in agreement with the analytical model. The simulation and model results are summarized in Fig. 5 where the excellent agreement is clearly seen.

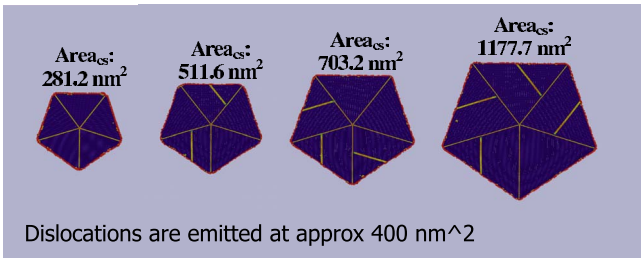

FIG. 4. (Color online) Relaxed structure of the multitwinned rods after high-temperature annealing showing how the increasing elastic strain is relieved by the emission of dislocations. The coloring is by centrosymmetry parameter showing the twin boundaries and the stacking faults created by the emission of partial dislocations.

To ensure the system finds the true global minimum energy in the simulations, we annealed the samples for 300 ps just below the melting temperature. The system is then cooled to 1 K in 350 ps and finally we perform the conjugate gradient minimization. We observed that for small cross-sectional areas below 450 nm^2 the structure on the far left of Fig. 7.4 is similar to the nonannealed sample shown in Fig. 3(a). However, when the nanorod area was greater than 450 nm^2 the potential energy caused by the elastic strain of 7.5° was large enough for a Shockley partial dislocation to be emitted, thus relieving the excess strain. Dislocations are expected to appear when the elastic energy equals the energy of a dislocation. Using our estimate of the elastic energy of $1/2G\varepsilon^2 A_{cs}L$ and making it equal to Gb^2L, we estimate the critical cross-sectional area for the emission of dislocations to be $2b^2/\varepsilon^2$. With $b = 0.29$ nm and $\varepsilon = 7.5/360$ we find the critical cross-sectional area to be 400 nm^2 in excellent agreement with the simulation results. As the cross-sectional area increased further, we observed a larger number of partial dislocations, as shown in the sequence of structures shown in Fig. 4. We note that the presence of dislocations in the MTR microstructures has also been observed in experimental studies.[12,17] The presence of dislocations relieves elastic energy and makes its contribution still smaller when compared to the excess energy due to the free surfaces of the rods.

The excess energy was calculated in the same way for the annealed and the nonannealed samples. The results of the simulations are shown in Fig. 5 including both the annealed and the nonannealed simulation excess energies as a function of cross sectional area. The results do not exhibit a significant change in the excess energy upon emission of the dis-

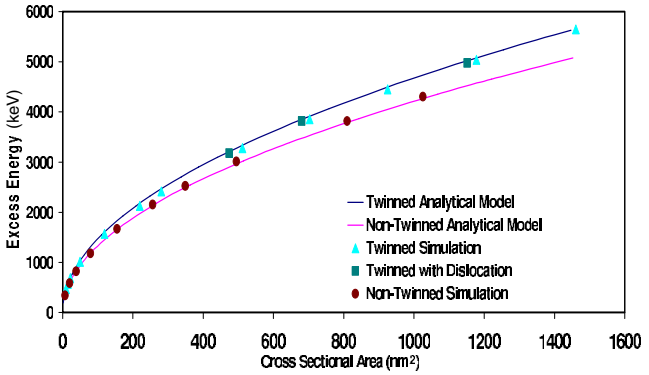

FIG. 5. (Color online) Excess energy of the twinned and nontwinned periodic nanorods as a function of the cross sectional area. The analytical models are represented by thick lines. The sample's axial length is 3.35 nm.

locations for this range of cross-sectional areas. We hypothesize that at larger sizes ($A_{cs} > 2000$ nm^2), the emission of dislocations will most likely be essential to the compensation of the high elastic strain and will play a larger role in the stability of the multitwinned nanorods. Note that neither the elastic or dislocation excess energies are included in the analytical model. The fact that the analytical model and the simulation results show excellent agreement confirms that the elastic energy term is indeed negligible for these cross sectional areas since it is by definition included in the simulations. The results of Fig. 5 confirm that the multitwinned periodic nanorods, without consideration of the energy due to the atomic structure of the end caps, are not stable at any size or aspect ratio. In Sec. VI, we modify our analytical model to incorporate the energetic contributions of the ends for both the multitwinned and nontwinned nanorods.

VI. ANALYTICAL MODEL FOR THE NANORODS INCLUDING THE ENDS

Having established the validity of our analytical model by comparison with the simulation results, we extend the analytical framework to incorporate the ends for the MTR and nontwinned structures. No new surface energy values are required in the extended model; all values are the same as those used in the Wulff construction and in the prior analytical model. To determine the end structures of the multitwinned nanorods we focused on experimental data. In particular, we choose the structure observed by Yacaman *et al.*[11] using TEM. The structures of the ends were found to be dipyramidal. The dipyramidal ends are made up of five (111) low-energy facets with a 30° slant, as shown in Fig. 6(a).[11] The analytical model includes the energy of the dipyramidal structure at both ends of the nanowire because the majority of experimental studies show growth along two dipyramidal ends.[7,9,12,20]

The ends are also considered for the nontwinned nanorod, which was assumed to be a truncated octahedron, consistent with the Wulff construction. The end structures for the nontwinned nanorod are shown in Fig. 6(b) and consist of two

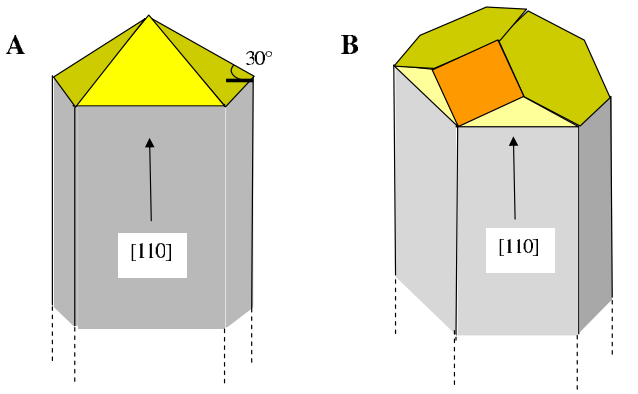

FIG. 6. (Color online) (a) Dipyramidal end of the multitwinned nanorod, as observed in Ref. 11. (b) The nontwinned nanorods with an end given by the Wulff construction. Hexagons and triangles (yellow) are [111] planes. Squares (orange) are [001] planes.

(001) square facets, two (111) hexagon facets, and four (111) triangle facets. The modified analytical model accounts for the geometry and surface energy of the nanorod ends.

The analytical excess energy of the ends of the MTR structures is given as a function of the cross-sectional area, A_{cs}, as shown

$$\Delta E_{\mathrm{MTR}}^{\mathrm{END}} = K_3 A_{cs}, \tag{8a}$$

where the constant K_3 is be defined as

$$K_3 = \frac{\gamma_3 \tan(\theta_1)}{\sin(\theta_1)\cos(\theta_4)}. \tag{8b}$$

With $\theta_1 = 0.628$ and $\theta_4 = 0.523$ and the surface energy found from the Wulff plot $\gamma_3 = \gamma_{111} = 1.6055$, we calculate the value $K_3 = 2.29$. Notice the excess energy of the multi twinned ends are linear with the cross sectional area, A_{cs}. The excess energy of the ends for the nontwinned nanorods is as follows:

$$\Delta E_{\mathrm{HEX}}^{\mathrm{End}} = K_4 A_{cs}. \tag{9a}$$

We define K_4 as

$$K_4 = \frac{\gamma_2\gamma_3 \sin(\theta_2)}{(\cos(\theta_3))^2}\left(\frac{\tan(\theta_4) + (\cos(\theta_4))^{-3}(\tan(\theta_4))^{-1} - 2\cos(\theta_3)(\cos(\theta_4))^{-2}}{2\gamma_3 \sin(\theta_3)\tan(\theta_3) + 2\gamma_3 \cos(\theta_3) - \gamma_2 \sin(\theta_2)\tan(\theta_3)}\right)$$
$$+ \frac{4\gamma_3^2}{\cos(\theta_3)(\cos(\theta_4))^2}\left(\frac{\cos(\theta_3) + \sin(\theta_3)\tan(\theta_3)}{4\gamma_3 \sin(\theta_3)\tan(\theta_3) + 4\gamma_3 \cos(\theta_3) - 2\gamma_2 \sin(\theta_2)\tan(\theta_3)}\right)$$
$$+ \frac{\gamma_2^2 \sin(\theta_2)}{(\cos(\theta_3))^2\cos(\theta_4)}\left(\frac{1}{2\gamma_3 \sin(\theta_3)\tan(\theta_3) + 2\gamma_3 \cos(\theta_3) - \gamma_2 \sin(\theta_2)\tan(\theta_3)}\right). \tag{9b}$$

The surface energies $\gamma_3 = \gamma_{111}$ and $\gamma_2 = \gamma_{001}$ are given in Table I. θ_2 and θ_3 are also defined in Table I and $\theta_4 = 30°$ is a geometric angle for the nontwinned nanorods, as seen in experiments. The calculated value for the constant K_4 when $\theta_2 = 1.57$, $\theta_3 = 2.53$, and $\theta_4 = 0.523$ with the surface energies equal to $\gamma_2 = \gamma_{001} = 1.7593$ and $\gamma_3 = \gamma_{111} = 1.6055$ is found to be $K_4 = 8.15$. A comparison of the constants K_3 and K_4 shows that $K_3 = 2.29$ is significantly lower than $K_4 = 8.15$ which in-

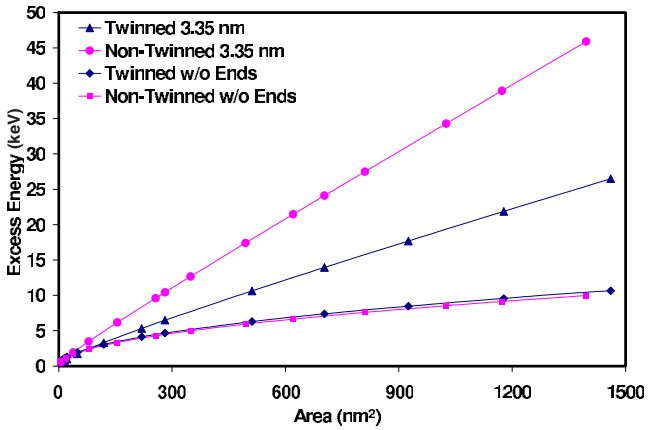

FIG. 7. (Color online) Results of the analytical model with and without the ends. The lengths of the nanorods are 3.35 nm. The data for the nanorods without ends are the same as Fig. 5.

dicates the contribution of the ends strongly favors the twinned nanorods. Figure 7 compares the excess energies of the multitwinned nanorods and nontwinned nanorods with and without ends for a total length of nanorod equal to 3.35 nm. When we include the influence of the ends on the system we see a dramatic difference in the energies of the system. The energy contribution of the ends increases linearly with the cross-sectional area and, as discussed below, the relative importance of the contribution from the ends to the total-energy balance depends on the aspect ratio of the rods.

A critical aspect ratio for the stability of the multitwinned structure can be calculated from the energetic condition, $[\Delta E_{\text{hex}}+\Delta E_{\text{hex}}(\text{end})] \geq [\Delta E_{\text{MTR}}+\Delta E_{\text{MTR}}(\text{end})]$. The equation for $\Delta E_{\text{hex}}(\text{total})=\Delta E_{\text{MTR}}(\text{total})$ is plotted in Fig. 8. The energy balance equation for the critical aspect ratio is given as

$$L = \frac{K_4 - K_3}{K_1 - K_2} A_{\text{cs}}^{1/2}. \tag{10}$$

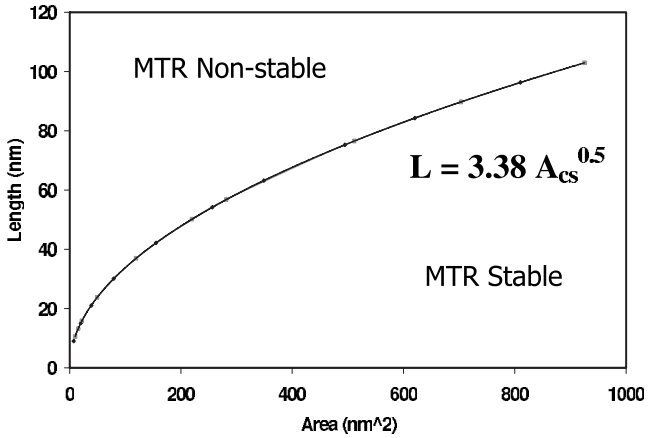

FIG. 8. Stability relationship between the length and the cross-sectional area given by $\Delta E_{\text{MTR}}=\Delta E_{\text{HEX}}$.

The critical aspect ratio, C, can be defined as the length divided by the square root of the cross sectional area. When the aspect ratio is below the critical value C, the MTRs are stable. The critical aspect ratio can be determined from the constants K_1, K_2, K_3, and K_4 given by Eqs. (5b), (7b), (8b), and (9b). These in turn depend on the various surface energies and the twin energy. To reiterate, the values found in our studies for the Voter-Chen potential are $K_1=7.05$, $K_2=5.32$, $K_3=2.29$, and $K_4=8.15$. The critical aspect ratio is calculated to be $C=(K_4-K_3)/(K_1-K_2)=3.38$. Figure 8 shows this condition in terms of a stability map, where length and cross-sectional area combinations lying below the curve represent energetically stable MTR configurations.

VII. DISCUSSION AND CONCLUSIONS

Through a combination of molecular dynamics, molecular statics, and an analytical model, we concluded that if the rod ends are not considered (i.e., periodic and infinite wires), multitwinned nanorods are not stable at any cross-sectional area. There was excellent agreement between the simulations and the analytical model developed, indicating that the model is indeed correct and that the elastic energy, not considered in the analytical model, is negligible for the cross-sectional areas studied here ($A_{\text{cs}}<1500$ nm^2). The analytical model was extended to include the ends of the nanorods. When the ends were introduced it was found that the existence of the ends was a major influence in the stability of the multitwinned nanorods. The energetics of the surface energy of the ends strongly favors the multitwinned structure, leading to a critical aspect ratio below which the MTR structure is stable.

Long nanorods have been produced experimentally through a number of growth mechanisms that focus on seed mediated growth.[8,12,14] These long nanorods start as small seeds with aspect ratios below the critical value. As the rods grow in length and surpass the critical value they become metastable. A transformation of a supercritical long multitwinned rod to the equilibrium structure given by the Wulff construction would clearly involve a large energy barrier.

The critical aspect ratio of 3.38 obtained in the present work is dependent on the particular values of the various surface energies given by the interatomic potential used here. Using the surface energies from a different interatomic potential, such as the Foiles-Baskes-Daw Ag EAM potential[30] in our analytical model, we obtained a critical aspect ratio of 4.16. Similarly, using the values given by the potential of Jiang-Min *et al.*,[31] we calculated a critical aspect ratio of 4.45. The experimental critical aspect ratio may vary slightly from these values because the interatomic potentials do not reproduce exactly the actual surface energies. Recent first principle calculations of the surface energy in Ag nanoparticles[32] indicate results that are in the range of 1.1–2 J/m^2, similar to the numbers that are obtained from EAM interatomic potentials.

In this study we focused on small cross sectional areas for which the elastic energy may be neglected when considering

the overall stability. These are the sizes relevant to the initial stages of growth of the nanorods from seeds, and the relative stability of the rods is entirely controlled by the surface and twin energies. The stability of the MTR for cross-sectional areas larger than ≈ 1500 nm^2 would require a more complex analytical model that incorporated the elastic energy and the presence of dislocations. In our studies we showed that dislocations can begin to form for cross sectional areas above 500 nm^2 although for these sizes their energetic contribution is still negligible when compared to the surface energy effects.

ACKNOWLEDGMENTS

This work was supported by NSF, Materials Theory program, and a portion of this work was performed at the Sandia National Laboratories, a multiprogram laboratory operated by Sandia Corporation, a Lockheed Martin company, for the National Nuclear Security Administration, DOE under Contract No. DE-AC04–94AL85000. The simulations were performed using System X, Virginia Tech's Supercomputer. We are grateful to Steve Plimpton for providing and maintaining the LAMMPS simulation code.

[1] B. Wu, A. Heidelberg, and J. Boland, Nat. Mater. **4**, 525 (2005).
[2] B. Wu, A. Heidelberg, J. J. Boland, J. Sader, X. Sun, and Y. Li, Nano Lett. **6**, 468 (2006).
[3] J. T. Hu, T. W. Odom, and C. M. Leiber, Acc. Chem. Res. **32**, 435 (1999).
[4] Y. Y. Yu, S. S. Chang, C. L. Lee, and C. R. C. Wang, J. Phys. Chem. B **101**, 6111 (1997).
[5] M. B. Mohamed, V. Volkov, S. Link, and M. A. El-Sayed, Chem. Phys. Lett. **317**, 517 (2000).
[6] C. J. Murphy and N. R. Jana, Adv. Mater. (Weinheim, Ger.) **14**, 80 (2002).
[7] Z. L. Wang, M. B. Mohamed, S. Link, and M. A. El-Sayed, Surf. Sci. Lett. **440**, L809 (1999).
[8] M. J. Yacamán, J. A. Ascencio, and G. Canizal, Surf. Sci. **486**, L449 (2001).
[9] H. Hofmeister, S. A. Nepijko, D. N. Ievlev, W. Schulze, and G. Ertl, J. Cryst. Growth **234**, 773 (2002).
[10] H. Chen, Y. Gao, H. Zhang, L. Liu, H. Yu, H. Tian, S. Xie, and J. Li, J. Phys. Chem. B **108**, 120238 (2004).
[11] J. Reyes-Gasga, J. L. Elechiguerra, C. Liu, A. Camacho-Bragado, J. M. Montejano-Carrizales, and M. Jose Yacaman, J. Cryst. Growth **286**, 162 (2006).
[12] H. Petrova, J. Perez-Juste, Z. Zhang, J. Zhang, T. Kosel, and G. V. Hartland, J. Mater. Chem. **16**, 3957 (2006).
[13] S. Ino, J. Phys. Soc. Jpn. **21**, 346 (1966).
[14] Y. Sun and Y. Xia, Science **298**, 2176 (2002).
[15] Y. Sun and Y. Xia, Adv. Mater. (Weinheim, Ger.) **14**, 833 (2002).
[16] Y. Sun, B. Mayers, T. Herricks, and Y. Xia, Nano Lett. **3**, 955 (2003).
[17] Y. Gao, P. Jiang, L. Song, L. Liu, X. Yan, Z. Zhou, D. Liu, J. Wang, H. Yuan, Z. Zhang, X. Zhao, X. Dou, W. Zhou, G. Wang, and S. Xie, J. Phys. D **38**, 1061 (2005).
[18] B. Wiley, Y. Sun, and Y. Xia, Langmuir **21**, 8077 (2005).
[19] C. Ni, P. A. Hassan, and E. W. Kaler, Langmuir **21**, 3334 (2005).
[20] J. Q. Hu, Q. Chen, Z. X. Xie, G. B. Han, R. H. Wang, B. Ren, Y. Zhang, Z. L. Yang, and Z. Q. Tian, Adv. Funct. Mater. **14**, 183 (2004).
[21] M. Liu and P. Guyot-Sionnest, J. Phys. Chem. B **109**, 22192 (2005).
[22] F. Ding, H. Li, J. Wang, W. Shen, and G. Wang, J. Phys.: Condens. Matter **14**, 113 (2002).
[23] L. D. Marks, Philos. Mag. A **49**, 81 (1984).
[24] A. F. Voter and S. P. Chen, in *Characterization of Defects in Materials*, MRS Symposia Proceedings No. 82, edited by R. W. Seigel, J. R. Weertman, and R. Sinclair (Materials Research Society, Pittsburgh, 1978), p. 175.
[25] S. K. Kwon, Z. Nabi, K. Kadas, L. Vitos, J. Kollar, B. Johansson, and R. Ahuja, Phys. Rev. B **72**, 235423 (2005).
[26] S. J. Plimpton, J. Comput. Phys. **117**, 1 (1995).
[27] V. V. Bulatov and W. Cai, *Computer Simulations of Dislocations*, 1st ed. (Oxford University Press, New York, 2006).
[28] B. Wiley, Y. Sun, B. Mayers, and Y. Xia, Chem.-Eur. J. **11**, 454 (2005).
[29] S. M. Foiles, Phys. Rev. B **49**, 14930 (1994).
[30] S. M. Foiles, M. I. Baskes, and M. S. Daw, Phys. Rev. B **33**, 7983 (1986).
[31] Z. Jian-Min, M. Fei, and X. Ke-Wei, Chin. Phys. **13**, 1082 (2004).
[32] B. Medasani, Y. H. Park, and I. Vasiliev, Phys. Rev. B **75**, 235436 (2007).